ITU Journal of Metallurgy and Materials Engineering

ITU/MMEJ

Thermal and Corrosion Properties of Binary Al-Ce Alloys

Sezgin Cengiz[1,2], Yunus Azakli[2,3], Kral Ali Cosan[2], Ebru Ceylan[4], Aytekin Uzunoglu[4,5], Mehmet Tarakci[2], Yucel Gencer[2]

[1] Department of Defense Technologies Institute, Gebze Technical University, 41400 Gebze, Kocaeli, Türkiye.
[2] Department of Materials Science and Engineering, Gebze Technical University, 41400 Gebze, Kocaeli, Türkiye.
[3] The Henry Royce Institute and Department of Materials Science and Engineering, The University of Sheffield, Sheffield, S1 3JD, United Kingdom.
[4] Metallurgical and Materials Engineering, Faculty of Engineering and Architecture, Necmettin Erbakan University, Konya, Türkiye.
[5] Department of Metallurgical and Materials Engineering, Faculty of Chemistry-Metallurgical Engineering, Istanbul Technical University, Istanbul, Türkiye.

Abstract: In this study, binary Al-xCe (x = 1, 2, 4, 8, 12, and 18 wt. %) alloys were synthesized, and the effect of cerium (Ce) on microstructures, thermal, and corrosion properties was systematically investigated. X-Ray diffraction (XRD) analyses revealed the presence of α-Al and $Al_{11}Ce_3$ phases in the alloys. The addition of Ce significantly reduced the coefficient of thermal expansion (CTE), decreasing from approximately 28.09 × 10^{-6} K^{-1} to 26.50 × 10^{-6} K^{-1}. The addition of Ce, especially at low concentrations, adversely affected the corrosion resistance of Al by introducing structural defects into the matrix. The increase in Ce content in the alloys led to an enhancement in its hardness.

Keywords: Aluminum, cerium, Al-Ce alloy, thermal expansion, corrosion.

İkili Al-Ce Alaşımlarının Termal ve Korozyon Özellikleri

Özet: Bu çalışmada, ikili Al-xCe (x = %1, 2, 4, 8, 12 ve 18 ağırlıkça) alaşımları sentezlenmiş ve seryum (Ce) ilavesinin mikroyapı, termal ve korozyon özellikleri üzerindeki etkisi sistematik olarak araştırılmıştır. XRD analizleri, alaşımlarda α-Al ve $Al_{11}Ce_3$ fazlarının varlığını ortaya koymuştur. Ce ilavesi, termal genleşme katsayısını (*TGK*) önemli ölçüde düşürmüş; bu değer yaklaşık 28,09 × 10^{-6} K^{-1}'den 26,50 × 10^{-6} K^{-1}'e gerilemiştir. Özellikle düşük konsantrasyonlarda Ce ilavesi, matris yapısına yapısal kusurlar oluşturarak Al'nin korozyon direncini olumsuz yönde etkilemiştir. Alaşımlardaki Ce içeriğinin artması ise sertlik değerinde bir artışa neden olmuştur.

Anahtar Kelimeler: Alüminyum, seryum, Al-Ce alaşımı, termal genleşme, korozyon.

Article

Corresponding Author: Sezgin Cengiz, E-mail: scengiz@gtu.edu.tr

Reference: Cengiz, S., Azakli, Y., Cosan, K.A., Ceylan, E., Uzunoglu, A., Tarakci, M. and Gencer, Y. (2025). Thermal and Corrosion Properties of Binary Al-Ce Alloys, *ITU Journal of Metallurgy and Materials Engineering*, 2(2), 31-36.

Submission Date : 7 July 2025
Online Acceptance : 26 July 2025
Online Publishing : 30 July 2025

1.Introduction

The automotive, aerospace, and transportation industries have been making significant efforts to design vehicles with consume lower fuel consumption in order to reduce energy used, especially to minimise harmful emissions that contribute air pollution. This challenge has driven the industry to increasingly use of aluminum alloys for structural components, owing to their lower density, high strength-density ratio (specific strength), possess good machinability, provide high corrosion resistance and are high recyclability. These characteristics render aluminum alloys a viable alternative to conventional steel, which is inherently limited by its relatively high density (Czerwinski, 2020, 2021; Wang et al., 1995; Zamani, 2015).

The high strength properties of the 2xxx series alloys, achieved by alloying aluminum with certain amounts of copper, the favorable mechanical properties of the magnesium-containing 5xxx series alloys, and better weldability and higher corrosion resistance of the magnesium-silicon-containing 6xxx series alloys have significantly increased the utilization of these materials in the automotive industry. The ability of aluminum alloys to exhibit excellent properties compared to denser steels and/or iron-based alloys has facilitated the development of lighter and more durable alternatives for components used in heavy-duty engine parts of vehicles (Chang et al., 2024; de Sousa Araujo et al., 2020; Fan et al., 2023; Van Der Hoeven et al., 2002).

In addition to enhancing the properties of existing aluminum alloys, researchers have continuously focused on developing new-generation technological alloys with tailored characteristics. In recent years, beyond the conventional alloying elements such as Cu, Si, Mg and Mn, Ce and Ni have been added as the main alloying elements in aluminum (Cengiz, 2020; Cengiz et al., 2023; Chang et al., 2024; de Sousa Araujo et al., 2020; Fan et al., 2023; Van Der Hoeven et al., 2002; Zamani, 2015). However, these elements are traditionally included among the conventional alloying elements of Al. Potentiodynamic corrosion tests have indicated that the introduction of Ce into the Al matrix has a detrimental effect on corrosion resistance. The highest corrosion potential and the lowest corrosion current were observed in unalloyed Al(Aydın, 2023; Zhu & Li, 2024).

The aim of this study is to investigate the effect of the Ce addition, in the range of 0.5 to 18 wt.%, on the microstructure as well as the thermal and mechanical properties of pure Al synthesized using an atmosphere-controlled induction system. A combination of experimental techniques was employed, including X-Ray diffraction (XRD), scanning electron microscopy (SEM) with energy-dispersive spectroscopy (EDS), and dilatometry.

2. Experimental

Binary Al-xCe (x = 1, 2, 4, 8, 12 and 18 wt.%) alloys were prepared using an atmosphere-controlled induction furnace using pure aluminum shot (99.9 %, Alfa Aesar) and pure Ce ingot (99.9 %). The alloys were melted in an alumina crucible and cast into copper mold with a rectangular cavity through an outlet at the bottom of the crucible. The cast ingots were sectioned, and the resulting samples were ground using SiC abrasive papers (320–1200 grit). Subsequently, the samples were polished using alumina and colloidal silica suspensions followed by cleaning with water and ethanol in an ultrasonic bath. XRD analysis of the alloys was carried out using Rigaku D-MAX 2200 and Bruker D8 diffractometers (40 kW, 40 mA) with Cu-Kα (λ = 1.5409 Å). The scans were conducted over a 2θ range of 10° to 90° with a step size of 0.05°.

Microstructural and elemental analysis of the alloys were conducted using a SEM FEI/Philips XL30 FEG ESEM equipped with EDS detectors. Vickers microhardness measurements were carried out using a Mitutoyo Micro Wizhard machine, applying a load of 500 g to the alloy surfaces. Cylindrical samples (5 mm diameter x 25 mm length) with a fine surface finish were prepared for dilatometric tests by machining sections from each ingot using a lathe and followed by grinding with 1200 grit abrasive papers. Linear expansion measurements were carried out using a Netzsch 402 PC dilatometer over the temperature range from room temperature (RT) to 450 °C of the alloys. Electrochemical corrosion tests were performed using a three-electrode setup, compromising consisting of an Ag/AgCl reference electrode, a Pt mesh as counter electrode and a working electrode connected to an Ivium Vertex One potentiostat. The tests were conducted in a 3.5 wt.% NaCl solution. The corrosion tests were conducted in a flat corrosion cell (Corrtest Instruments CS936) with an Ag/AgCl reference electrode and a built-in Pt mesh counter electrode. The exposed sample area was 1 cm^2. The samples were submerged into the electrolyte for 1h before the experiments for potential stabilization. The tests were conducted at a scan rate of 1 mV/s (Chen et al., 2024; Noori et al., 2025).

3. Results and Discussion

3.1. Phase Composition of Al-Ce Alloys

The XRD spectrums obtained from the surface of alloys are given in Figure 1. The diffraction patterns reveal the presence of α-Al (PDF #01-089-3657) and $Al_{11}Ce_3$ (orthorhombic, PDF #00-019-0006) phases in all as-cast hypo- and hyper-eutectic Al-Ce alloys. The XRD patterns clearly illustrate how the peak intensities in as-cast metallic samples can differ from standard powder diffraction patterns. For example, in pure aluminum powder patterns, the most intense peak typically appears at 2θ = 38.4°, corresponding to the (111) plane. However, in the present study, the aforementioned peak exhibited notably lower intensity than those observed at 45° (200), 65° (220) and 78° (311). This deviation can be attributed to preferential crystallographic orientation of the Al grains on the analysed surface. Furthermore, the intensity of the peaks corresponding to the $Al_{11}Ce_3$ phase increased with increasing Ce content which is consistent with the expected increase in the volume fraction of the $Al_{11}Ce_3$ phase as more cerium is introduced into the alloy.

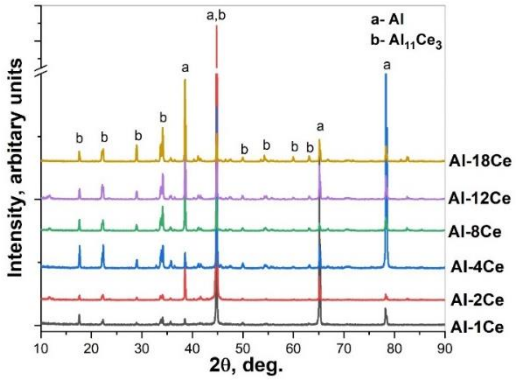

Figure 1. XRD spectrum of the as-cast Al-Ce alloys.
Şekil 1. Döküm Al-Ce alaşımlarının XRD spektrumu.

3.2. Microstructure, Elemental Distribution and Microhardness of Al-Ce Alloys

The microstructure of the as-cast Al-Ce alloys are shown in Figure 2. and Figure 3. These microstructural images provide a better understanding of the quantity and distribution of intermetallic phases in the alloys, offering complementary information to the XRD analysis.

The hypoeutectic Al-1Ce, Al-2Ce, Al-4Ce, Al-8Ce alloys exhibited a typical dendritic microstructure, which is commonly observed in many as-cast alloys (Figure 2a-d)(Sims et al., 2017; Weiss, 2019; Weiss et al., 2017). In these compositions, the dendritic region with dark grey contrast correspond to the proeutectic Al while the interdendritic region display a lighter appearance and a lamellar morphology, consisting of eutectic α-Al (dark grey lamellae) and eutectic $Al_{11}Ce_3$ (white lamellae).

As the Ce content increases, the volume fraction of lamellar structure -and therefore the eutectic $Al_{11}Ce_3$ phase- also increases noticeably. The alloys with hypereutectic compositions (Al-12Ce, Al-18Ce) exhibited blocky light appearing primary $Al_{11}Ce_3$ crystals, in addition to lamellar eutectic structure composed of $Al_{11}Ce_3$ and Al as well as a small volume of dendritic Al (dark grey) (Figure 2e, f). The primary eutectic $Al_{11}Ce_3$ phases in these alloys appear as truncated rods with square cross-sections, particularly pronounced in the Al-18Ce alloy, where their volume fraction is noticeably higher. The transition in microstructure between hypoeutectic and hypereutectic compositions is illustrated in detail in Figure 3.

In Fig 3b, the blocky primary $Al_{11}Ce_3$ crystal is surrounded by the $Al/Al_{11}Ce_3$ eutectic structure and residual Al dendrites. For hypereutectic compositions, under ideal cooling conditions, solidification starts with the nucleation and growth of the primary $Al_{11}Ce_3$ phase which continues until the system reaches the eutectic temperature. Then, below the eutectic reaction temperature, the remaining liquid phase transforms into eutectic $Al/Al_{11}Ce_3$ structure. It has been reported that a high degree of undercooling can shift eutectic composition towards the higher solute content side and cause the eutectic reaction to occur at lower temperatures (Abboud & Mazumder, 2020; CENGİZ, 2020).

In a study on the $Al/Al_{11}Ce_3$ eutectic transformation in hypo- and hypereutectic Al-Ce alloys cast in steel molds. Al dendrites were observed in all hypereutectic compositions (Al-11Ce, Al-12Ce, Al-15Ce, Al-20Ce). Therefore, the presence of Al dendrites in the microstructure of hypereutectic alloys can be attributed to a high degree of undercooling which is likely intensified by the use of a copper casting mold (CENGİZ, 2020; Czerwinski & Amirkhiz, 2020).

It has been reported that the hypoeutectic Al-Ce alloys consisted of well-aligned lamellae of Al and $Al_{11}Ce_3$.The initially parallel lamellar structures gradually transform into L-shaped, C-shaped and eventually U-shaped $Al_{11}Ce_3$ with increasing of Ce content in alloys (Czerwinski & Amirkhiz, 2020). However, these previously reported morphologies were not t observed in the SEM images of the hypereutectic Al-Ce alloys even under high magnification (Figure 3d). Although the $Al/Al_{11}Ce_3$ eutectic structures are described in the literature as consisting of parallel lamellae, such arrangements were not evident in the examined hypereutectic samples (CENGİZ, 2020; Czerwinski & Amirkhiz, 2020). However, it has been reported that the eutectic morphology depends on the Ce content, with hypoeutectic alloys typically exhibiting a lamellar structure, while increasing Ce concentration leads to the formation of L-shaped and C-shaped morphologies (CENGİZ, 2020; Czerwinski & Amirkhiz, 2020; Weiss et al., 2017). Elementals analysis results are given in Figure 4. According to point elementals analysis, the Al matrix marked as “1” exhibited negligible Ce solubility. It has been reported that the solubility of Ce in Al is very low, reaching up to only 0.01 at. % Ce (0.05 wt. % Ce) at 640 °C (Sims et al., 2017). In Figure 4, the region marked with “2” corresponds to the proeutectic $Al_{11}Ce_3$ phase. The EDS results obtained from this region are consistent with the expected composition of the $Al_{11}Ce_3$ phase (Figure 4c).

In another study, phase estimations were made using computer-aided calculation methods, reporting an even lower Ce solubility in Al at 0.0001 wt. % (Sims et al., 2017). In Figure 4, the region marked as “2” corresponds to the proeutectic $Al_{11}Ce_3$ phase. The SEM-EDS results obtained from this region are consistent with the expected composition of the $Al_{11}Ce_3$ phase (Figure 4c). Figure 5 shows the microhardness values calculated from the indentation dimensions measured using optic microscopy.

The highest hardness value of 62 HV was measured in the Al-18Ce alloy and that the hardness of as-cast Al–Ce alloys increase with Ce content, ranging from about 25 HV to 62 HV for compositions with 1 to 18 wt. % Ce. Another study reported that the hardness of $Al_{11}Ce_3$ intermetallic is approximately 350 HV. (Cengiz, 2020; CENGİZ, 2020).

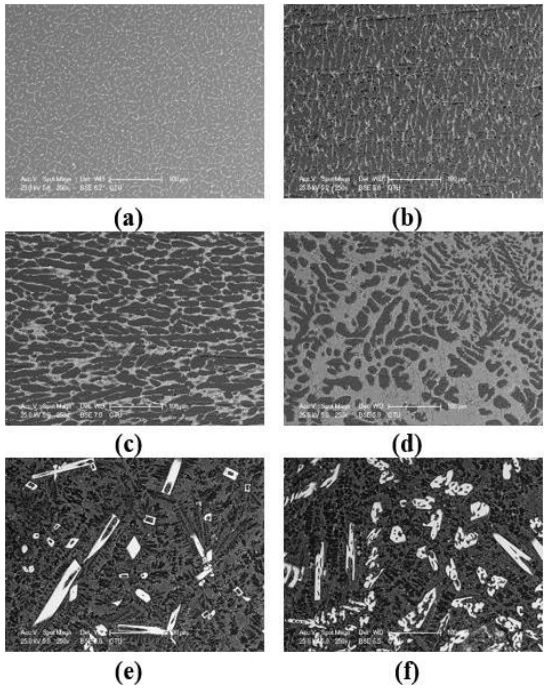

Figure 2. SEM micrographs of Al-Ce alloys with varying Ce content, (a) Al-1Ce, (b) Al-2Ce, (c) Al-4Ce, (d) Al-8Ce, (e) Al-12Ce, (f) Al-18Ce.

Şekil 2. Değişen Ce içeriğine sahip Al-Ce alaşımlarının SEM görüntüleri, (a) Al-1Ce, (b) Al-2Ce, (c) Al-4Ce, (d) Al-8Ce, (e) Al-12Ce, (f) Al-18Ce.

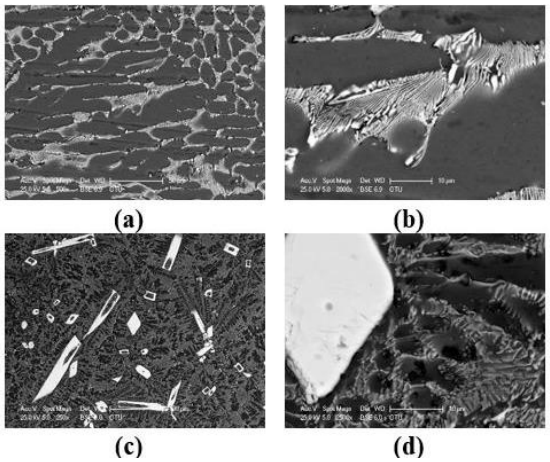

Figure 3. SEM micrographs of Al-Ce alloys: (a) Al-4Ce, (b) high magnification view of Al-4Ce, (c) Al-12Ce, and (d) high magnification view Al-12Ce.

Şekil 3. Al-Ce alaşımlarının SEM görüntüleri: (a) Al-4Ce, (b) Al-4Ce'nin yüksek büyütmede görünümü, (c) Al-12Ce ve (d) Al-12Ce'nin yüksek büyütmede görünümü.

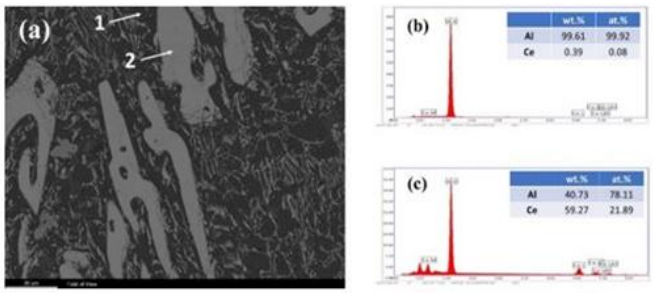

Figure 4. SEM micrographs of Al-18Ce and SEM-EDS elemental analysis of the microstructure of the Al-18Ce alloy at different points shown in Figure 4a: (a) SEM image, (b) analysis at point 1, and (c) analysis at point 2.

Şekil 4. Al-18Ce alaşımına ait SEM mikrografları ve Şekil 4a'da gösterilen farklı noktalardaki mikroyapıya ait SEM-EDS elementel analizleri: (a) SEM görüntüsü, (b) 1. noktadaki analiz, (c) 2. noktadaki analiz.

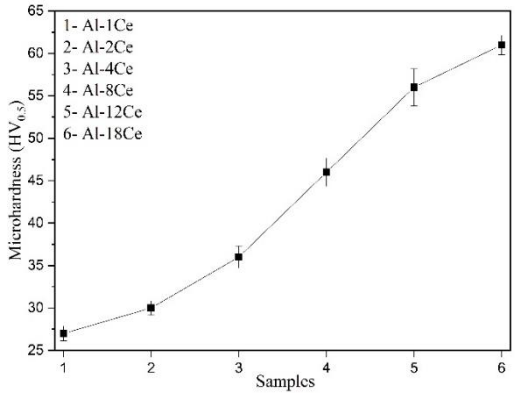

Figure 5. Microhardness measurement results of the alloys.

Şekil 5. Alaşımların mikrosertlik ölçüm sonuçları.

3.3. Thermal Expansion Behaviour of As-Cast Al-Ce Alloys

Linear thermal expansion curves and coefficient of thermal expansion of the as-cast Al-Ce alloys are presented in Figure 6. The CTE values decrease with increasing Ce content in alloys. The CTE is reduced significantly from approximately 28.09 × 10-6 K^{-1} to 26.50 × 10^{-6} K^{-1} as the Ce content reaches 8 wt. % and above. This reduction is attributed to the formation of thermally stable Al-Ce intermetallic phases (Cengiz et al., 2023).

Cerium exhibits extremely low solubility in aluminum (~0.005 wt. % at room temperature) and reacts with Al to form binary intermetallic compounds that are stable at elevated temperatures(Czerwinski & Amirkhiz, 2020; Sims et al., 2017). Additionally, the diffusivity of Ce in Al is remarkably low due to its large atomic radius. For example, the diffusion coefficient of Ce at 500 °C is 5.7 × 10^{-14} cm^2/s, which is nearly 10,000 times lower than that of Cu (6.0 × 10^{-10} cm^2/s) or Mg (1.4 × 10^{-9} cm^2/s). This low diffusivity contributes to the high thermal stability of the alloy (Du et al., 2003).

The Al-Ce system exhibits a eutectic reaction that results in the formation of two intermetallic phases: α- $Al_{11}Ce_3$ and β-$Al_{11}Ce_3$. The α-phase transforms into the β-phase above 1006 °C, with the β-phase having a melting point of 1253 °C. In contrast, pure aluminum has a relatively low melting point of ~660 °C, which limits its applicability in high-temperature environments. However, the presence of these high-melting intermetallic compounds (~1200 °C) significantly enhances the alloy's thermal stability. Intermetallic phases and second-phase particles, such as nanoparticles, are known to improve both the mechanical properties and thermal resistance of alloys. The stability of these phases is closely related to their melting points and diffusion coefficients, which are critical parameters for maintaining structural integrity at elevated service temperatures over extended periods (Cengiz et al., 2023; Czerwinski, 2020; Gao et al., 2005; Sims et al., 2017; Weiss, 2019).

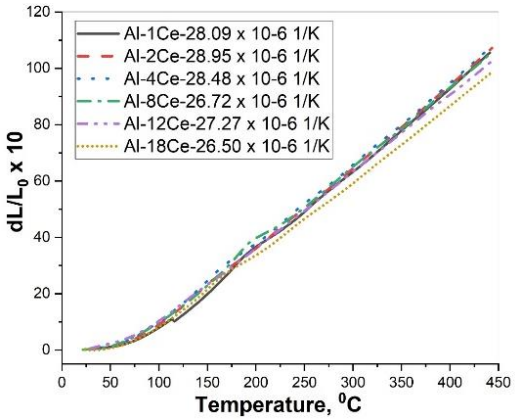

Figure 6. Coefficient of thermal expansion curves of the as-cast Al–Ce alloys, along with the corresponding CTE values evaluated at 400 °C.

Şekil 6. Döküm Al-Ce alaşımlarının termal genleşme katsayısı (TGK) eğrileri ve 400°C'deki TGK değerleri.

3.4. Corrosion Properties of As-Cast Alloys

The corrosion properties of the alloys were determined using a 3-electrode setup in which an Ag/AgCl reference electrode and Pt mesh were used. The experiments were conducted in 3.5 wt.% NaCl at room temperature. To reach the equilibrium, before the experiments the samples were immersed in the electrolyte for a certain amount of time. The measured corrosion parameters are listed in Table 1. Figure 7 shows the potentiodynamic polarization curves of the prepared alloys with varying Ce content. The results revealed the effect of Ce content on the corrosion resistance of Al obviously. While the corrosion potential of pristine Al was measured as -0.758 V, the addition of 1% of Ce into the structure decreased the corrosion potential to -1.3 V. It should be noted that the corrosion potential is a thermodynamic property. In addition, the smaller corrosion potential indicates the greater tendency for corrosion (Zhang et al., 2022). On the other hand, the corrosion current is associated with the reaction kinetics, and the larger value indicates higher corrosion rate. Based on that information, the values given Table 1 implies that the addition of Ce into the Al phase resulted in a detrimental effect on the corrosion property compared to the pristine Al. On the other hand, it will be wise to discuss that the highest impact was observed on the introduction of small Ce content, which might be attributed to the defective effect of Ce in the Al matrix. The finding is compatible with the results, showing the alloying effects of Ce in the Al matrix (Zhou & Xiong, 2022).

Table 1. Corrosion parameters of Al and Ce-modified Al samples.

Tablo 1. Al ve Ce-modifiyeli Al numunelerinin korozyon parametreleri.

Sample	Icorr (μA/cm²)	Ecorr (mV)
Pristine Al	2.65	-758.0
Al-1Ce	20.90	-1300
Al-2Ce	45.40	-918.0
Al-4Ce	43.10	-893.0
Al-8Ce	25.90	-882.0
Al-12Ce	35.30	-893.0
Al-18Ce	9.08	-811.0

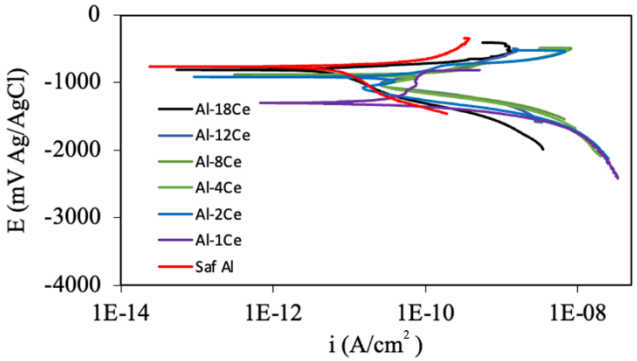

Figure 7. Potentiodynamic polarization curves of Al-Ce alloys.
Şekil 7. Al-Ce alaşımlarının potansiyodinamik polarizasyon eğrileri.

4. Conclusion

The study focused on the influence of Ce content in binary Al-Ce alloys on the microstructure, and the thermal and corrosion properties of the alloys.

- CTE values decreased progressively with the increasing addition of Ce.
- The progressive increase in Ce content in the alloy resulted in a corresponding enhancement in hardness.
- The addition of Ce to Al adversely affected its corrosion resistance, as indicated by a shift to more negative corrosion potentials and increased current densities. The most significant impact was observed at low Ce content, likely due to structural defects introduced in the Al matrix.

5. Acknowledgements

Acknowledges financial support of Gebze Technical University through the program number BAP A105-61. The authors would like to express their thanks to technicians Ahmet Nazim and Adem Sen for their technical assistance in performing the analytical measurements during the experimental SEM, EDS, and XRD studies.

6. Conflicts of Interest

The authors declared that there is no conflict of interest to this work. The work is in its current state is original, unpublished and not being considered for publication elsewhere.

7. References

Abboud, J., & Mazumder, J. (2020). Developing of nano sized fibrous eutectic silicon in hypereutectic Al–Si alloy by laser remelting. *Scientific Reports*, *10*(1). https://doi.org/10.1038/s41598-020-69072-1

Aydın, F. (2023). A review of recent developments in the corrosion performance of aluminium matrix composites. In *Journal of Alloys and Compounds* (Vol. 949). https://doi.org/10.1016/j.jallcom.2023.169508

CENGİZ, S. (2020). Farklı Miktarlarda Seryum ve Silisyum İçeren Alüminyum Alaşımlarının Karşılaştırılması. *Bilecik Şeyh Edebali Üniversitesi Fen Bilimleri Dergisi*, *7*(2). https://doi.org/10.35193/bseufbd.723326

Cengiz, S. (2020). Synthesis of eutectic Al–18Ce alloy and effect of cerium on the PEO coating growth. *Materials Chemistry and Physics*, *247*. https://doi.org/10.1016/j.matchemphys.2020.122897

Cengiz, S., Aboulfadl, H., & Thuvander, M. (2023). Effect of Ce addition on microstructure, thermal and mechanical properties of Al-Si alloys. *Materials Today Communications*, *34*. https://doi.org/10.1016/j.mtcomm.2023.105518

Chang, Z., Liu, L., Sui, Z., Yan, X., Li, Y., Zhang, Y., Zhang, Y., & Yang, M. (2024). Effect of Aging Temperature on Pitting Corrosion of AA6063 Aluminum Alloy. *Metals and Materials International*, *30*(6). https://doi.org/10.1007/s12540-023-01587-4

Chen, X., Wang, Z., Yu, S., & Li, G. (2024). Corrosion inhibition of carbon steel in NaCl solution Using a mixture of alkanol amine and calcium nitrite: Electrochemical and microscopic evaluation. *International Journal of Electrochemical Science*, *19*(11), 100802. https://doi.org/https://doi.org/10.1016/j.ijoes.2024.100802

Czerwinski, F. (2020). Thermal stability of aluminum alloys. In *Materials* (Vol. 13, Issue 15). https://doi.org/10.3390/ma13153441

Czerwinski, F. (2021). Current trends in automotive lightweighting strategies and materials. *Materials*, *14*(21). https://doi.org/10.3390/ma14216631

Czerwinski, F., & Amirkhiz, B. S. (2020). On the Al-Al11Ce3 eutectic transformation in aluminum-cerium binary alloys. *Materials*, *13*(20). https://doi.org/10.3390/ma13204549

de Sousa Araujo, J. V., Milagre, M. X., Ferreira, R. O., de Souza Carvalho Machado, C., de Abreu, C. P., & Costa, I. (2020). Microstructural Characteristics of the Al Alloys: The Dissimilarities Among the 2XXX Alloys Series used in Aircraft Structures. *Metallography, Microstructure, and Analysis*, *9*(5). https://doi.org/10.1007/s13632-020-00688-5

Du, Y., Chang, Y. A., Huang, B., Gong, W., Jin, Z., Xu, H., Yuan, Z., Liu, Y., He, Y., & Xie, F.-Y. (2003). Diffusion coefficients of some solutes in fcc and liquid Al: critical evaluation and correlation. *Materials Science and Engineering: A*, *363*(1–2), 140–151.

Fan, S., Chen, M., Jiang, K., Lan, Y., & Rong, G. (2023). The effects of Cu and Mg contents on the thermal stability of 6XXX-series aluminum alloy. *Advances in Mechanical Engineering*, *15*(1). https://doi.org/10.1177/16878132221148909

Gao, M. C., Ünlü, N., Shiflet, G. J., Mihalkovic, M., & Widom, M. (2005). Reassessment of Al-Ce and Al-Nd binary systems supported by critical experiments and first-principles energy calculations. *Metallurgical and Materials Transactions A: Physical Metallurgy and Materials Science*, *36*(12). https://doi.org/10.1007/s11661-005-0001-y

Noori, Mohsen., yousefpour, Mardali., Abdollah-Pour, Hassan., & Pishbin, Hassan. (2025). Influence of current density on the microstructure and corrosion resistance of PEO coatings on pure Zr. *Results in Engineering*, *26*, 105204. https://doi.org/https://doi.org/10.1016/j.rineng.2025.105204

Sims, Z. C., Rios, O. R., Weiss, D., Turchi, P. E. A., Perron, A., Lee, J. R. I., Li, T. T., Hammons, J. A., Bagge-Hansen, M., Willey, T. M., An, K., Chen, Y., King, A. H.,

& McCall, S. K. (2017). High performance aluminum-cerium alloys for high-temperature applications. *Materials Horizons*. https://doi.org/10.1039/c7mh00391a

Van Der Hoeven, J. A., Zhuang, L., Schepers, B., De Smet, P., & Baekelandt, J. P. (2002). A new 5xxx series alloy developed for automotive applications. *SAE Technical Papers*. https://doi.org/10.4271/2002-01-2128

Wang, L., Makhlouf, M., & Apelian, D. (1995). Aluminium die casting alloys: Alloy composition, microstructure, and properties-performance relationships. *International Materials Reviews*. https://doi.org/10.1179/imr.1995.40.6.221

Weiss, D. (2019). Improved High-Temperature Aluminum Alloys Containing Cerium. In *Journal of Materials Engineering and Performance*. https://doi.org/10.1007/s11665-019-3884-2

Weiss, D., Rios, O., Sims, Z., McCall, S., & Ott, R. (2017). Casting Characteristics of High Cerium Content Aluminum Alloys. *Minerals, Metals and Materials Series*, *0*. https://doi.org/10.1007/978-3-319-51541-0_28

Zamani, M. (2015). *Al-Si Cast Alloys -Microstructure and Mechanical Properties at Ambient and Elevated Temperature*. Jönköping University.

Zhang, X., Sui, Y., Jiang, Y., & Wang, Q. (2022). Effect of Ce on the Microstructure and Corrosion Resistance of Al-5Mg-3Zn-1Cu Alloy. *Metals*, *12*(3). https://doi.org/10.3390/met12030371

Zhou, X., & Xiong, H. (2022). Corrosion behavior of Al-Ce alloys in 3.5%NaCl solution. *International Journal of Electrochemical Science*, *17*. https://doi.org/10.20964/2022.02.06

Zhu, H., & Li, J. (2024). Advancements in corrosion protection for aerospace aluminum alloys through surface treatment. In *International Journal of Electrochemical Science* (Vol. 19, Issue 2). https://doi.org/10.1016/j.ijoes.2024.100487